

# Incident beam diffraction in electron-stimulated desorption: Theory and experiment

M. T. Sieger, G. K. Schenter, and T. M. Orlando

*W. R. Wiley Environmental Molecular Sciences Laboratory*

*Pacific Northwest National Laboratory, P.O. Box 999, MSIN K8-88, Richland, WA 99352*

J. J. Rehr

*Department of Physics (FM-15), University of Washington, Seattle, Washington 98195*

(July 9, 1999)

## Abstract

We derive a mathematical expression for the effect of incident beam diffraction on inelastic electron-surface interactions. We present a method, based upon the separable-propagator multiple-scattering cluster formalism of Rehr and Albers, for calculating incident beam diffraction in electron-surface interactions. The cluster-based calculations are suitable for periodic or non-periodic systems. We discuss the application of this model to several cases in which surface probes in which incident beam diffraction has been observed experimentally, including secondary electron emission, Auger electron spectroscopy, and electron-stimulated desorption.

79.20.La 61.14.Rq 79.60.Dp 61.14.Dc

Typeset using REVTEX

## I. INTRODUCTION

Electron-stimulated desorption (ESD) is a process of great interest for many diverse disciplines, including astrophysics [ ] and semiconductor device processing [ ]. Excitations in a solid, caused by an incident beam of electrons, lead to the ejection of ions, neutral atoms, or molecules from a surface. Currently popular models of ESD describe the desorption process with a two-step model, in which the total ESD cross section is written, where  $\sigma$  is the excitation (inelastic electron-solid scattering) cross-section and  $P$  is the total desorption or escape probability. The total desorption rate is then the incident electron flux times the total ESD cross section. The vast majority of effort in experimental and theoretical ESD has focused on the desorption probability, and its effect on the final-state kinetic energy and/or desorption trajectory distributions. However, there are initial-state effects in ESD which can have a large impact on the desorption yield, independent of the desorption probability. One possible initial state effect is elastic scattering of the incident electron.

two factors as being the most important affecting ESD cross-sections [ ]. These factors are, to first order, independent of the direction of the incident electron beam. However, at the energies of interest for most ESD ion thresholds (10-100 eV), the elastic electron scattering amplitudes in the solid are large, and are comparable to the inelastic scattering cross-sections. (Note - is this strictly true? ) The strength of elastic scattering is the basis for such well-known experimental techniques as low-energy electron diffraction (LEED) and photoelectron diffraction (PED). The interference of the elastically scattered electron amplitudes with the direct (or unscattered) amplitude can be thought of as a standing wave at the surface in a time-independent picture, with spatially localized maxima and minima in the incident electron density. Since the probability of the inelastic scattering event which leads to desorption is proportional to the incident electron density at the absorber, the ESD cross section can depend upon the local atomic structure and the k-vector of the incident wave.

Electron diffraction has been observed to affect the desorbate yields in photon-stimulated

desorption (PSD) measurements, through the extended x-ray absorption fine structure (EX-AFS) effect [ ]. Jaeger et. al. reported SEXAFS oscillations in the yield of O+ ions liberated from a O/Mo(100) surface under synchrotron UV illumination. The SEXAFS measured in this way gives data equivalent to traditional X-ray absorption spectroscopy, and structural information in the form of bond-lengths can be extracted.

The yield of H+ ions from a Pd(111) crystal was observed by Drube et. al. to follow the total electron yield in x-ray standing wave (XSW) measurements [ ]. Since the XSW technique relates the electron yield to local structure, it was suggested that total ion yields could also be used to gather structural information. However, this result has not been followed up on, primarily because of concerns for the effect of secondary electrons, of which there are many due to the KeV incident energies.

The total desorption yield, when measured as a function of incident  $k$ , carries information about the bonding geometry of the desorbate before excitation - this is an important distinction from ESD ion angular distributions (ESDIAD), which measures the desorption trajectories of the excited species, and may not necessarily reflect the true ground state bonding geometry. This electron standing-wave stimulated desorption (ESW-SD), then, can be used as a surface structure probe similar to the popular x-ray standing wave technique, in which an incident photon forms a spatially-varying field in the solid.

In Section II we present a multiple-scattering theory of electron diffraction effects in ESD, based upon the separable propagator of Rehr and Albers [ ], and describe a surface analysis technique taking advantage of diffraction in ESD, which we call electron standing-wave stimulated desorption (ESW-SD). In Section III we will present theoretical calculations of ESW amplitudes for some model systems, and in Section IV we will discuss the experimental implementation of these ideas, and present measurements of ESW-SD in the F+/Si(100) and H+/Si(100) systems.

The collision process between an electron and a surface atom is an isolated event, meaning that a one-electron theory of the collision process is a

Efforts to perform quantitative surface structure measurements with ESD have focused

upon ESDIAD, which gives information about the desorbate bond-axis directions, but only indirectly. A difficulty with performing quantitative analysis of ESDIAD data is that the desorbate evolves on a final state potential surface which is very complex, and can alter the desorbate trajectories. Since detailed information about the final state potentials is usually lacking, ESDIAD has been primarily restricted to qualitative or, at best, semi-quantitative analysis.

The ESW-SD technique, however, is a purely initial-state effect, and should not suffer from as many unknown quantities as ESDIAD. The success of LEED, EXAFS, and PED calculations in general give us confidence that real quantitative structural information can be gained from careful ESW-SD measurements, and therefore ESW-SD represents a significant advance in the usage of ESD for surface structure determination.

Many materials analysis techniques utilize electron beams to probe the electronic, geometric, and chemical properties of surfaces. Electrons with kinetic energies in the range of 10 - 1000 eV are a choice probe for surface analysis because of their very short mean free path in solids (on the order of 10 Å)<sup>1</sup>. The wavelength of low-energy electrons (1.2 Å at 100 eV) is on the order of the distance between individual atoms in molecules and solids, and electron diffraction is widely used as a probe of surface geometry on the atomic scale.

The different types of electron-surface spectroscopies can be separated into two broad classes; elastic (with a change of momentum but without change of energy) and inelastic (with a change of energy). The most well-known elastic surface probe is low-energy electron diffraction (LEED)<sup>4</sup>, but this class also includes reflection high-energy electron diffraction (RHEED) and transmission electron diffraction (TED). Inelastic electron probes include electron energy loss spectroscopy (EELS), Auger electron spectroscopy (AES) and Auger electron diffraction (AED), secondary electron emission (SEE), electron stimulated desorption (ESD), cathodoluminescence, e-2e spectroscopy<sup>3</sup>, and numerous variations on these techniques.

Inelastic probes use the incident electron to generate excitations in the solid, and spectroscopy is performed on the products of the excitation. Differences in the various techniques

lie in the energy of electron and the mode of product detection. AES, SEES, and EELS, secondary (or inelastically scattered primary) electrons are detected. In ESD, ions created at the surface and desorbed from the solid are detected. In all of these cases, the phenomenon is initiated by the inelastic scattering of the primary electron by atoms in the solid.

It has been observed in numerous investigations that elastic scattering and interference of the incident electron beam in the initial state can have a measurable impact on the quantity of interest. For example, it has been known for many years that the yield of secondary electrons emitted from a crystalline solid depends not only upon the primary electron energy, but also on the angle of incidence with respect to the crystal symmetry axes ??, and has been described as an inverse Kikuchi effect (or inverse channeling of electrons). Incident beam diffraction has also been observed to affect the Auger emission process. Diffraction of the incident electron is an important process, and is necessary to understand for a quantitative understanding of electron spectroscopies. where knowledge of incident beam diffraction (IBD) effects is necessary for the quantitative interpretation of data.

The concept of surface analysis utilizing incident beam interference forms the basis of the x-ray standing wave (XSW) technique. X-ray standing wave induced fluorescence has been used to holographically image bulk crystal structure [reference here].

This article considers the role of incident electron diffraction in the inelastic scattering of electrons from solid surfaces, and is presented in two parts. In Part I, we present a theory of incident beam diffraction in inelastic electron-surface spectroscopies, and discuss sample calculations and implications for secondary electron emission and Auger electron spectroscopy. In Part II, we discuss experimental measurements and calculations of incident beam diffraction in electron-stimulated desorption.

Our primary interest is to calculate the effect of incident beam diffraction on the total excitation rate. Interference of the direct amplitude with waves elastically scattered from the crystal lattice forms an electron "standing wave", with spatially localized maxima and minima in the incident electron density. Whether a particular point on a surface experiences a maximum or minimum depends on the wavelength of the electron, the direction of incidence

relative to the crystal axes, and the local arrangement of atoms in the lattice (see Figure 1(a)). Since the probability of excitation is proportional to the incident electron density at the site of the "absorber" (the site of the electronic excitation), the total excitation rate should depend upon the local atomic structure and the k-vector of the incident wave.

## II. THEORY

### A. Interaction picture

We will use throughout this paper Hartree atomic units,  $\hbar = e = m_e = 1$ . The fundamental quantity of interest is the rate at which excitations are caused in the solid by the incident electron beam. By Fermi's golden rule, the excitation rate is

$$R_{if} = 2\pi|M_{if}|^2\rho_i\rho_f\delta(E_f - E_i), \quad (1)$$

where  $\rho_{i,f}$  is the density of initial and final states, and the  $\delta$ -function conserves the total system energy. The transition matrix elements  $M_{if}$  are given by

$$M_{if} = \langle\psi_f\phi_f|V|\psi_i\phi_i\rangle, \quad (2)$$

where  $\psi_{i,f}$  and  $\phi_{i,f}$  are the initial and final state wavefunctions of the solid and the incident electron, respectively. The proper form of the bra and ket in equation 2 are Slater determinants of solutions to the Schrödinger equation in the presence of the full potential of the solid.

The integral in Eq. 2 is very challenging to perform. To make the problem tractable, various approximations are necessary. The first approximation we make is to assume single-particle wavefunctions  $\psi_{i,f}(\mathbf{r})$  for the solid, with energies  $\epsilon_i$  and  $\epsilon_f$ . We then assume that the interaction carrying the solid from the initial to the final state is driven by the charge density presented by the incident electron in its initial state;

$$M_{if} \propto \langle\psi_f(\mathbf{r})|\int \frac{e^{-a|\mathbf{r}-\mathbf{r}'|}}{|\mathbf{r}-\mathbf{r}'|}\rho(\mathbf{r}')d\mathbf{r}'|\psi_i(\mathbf{r})\rangle, \quad (3)$$

where  $\rho(\mathbf{r}') = \phi^*(\mathbf{k}_i, \mathbf{r}')\phi(\mathbf{k}_i, \mathbf{r}')$  is the initial state charge density of the incident electron, and  $V$  in Eq. 2 has been replaced by a screened Coulomb potential with screening length  $a^{-1}$ . In essence, this initial state density approximation is equivalent to an impulse approximation, and assumes that the excitation rate is independent of the details of the final state of the incident electron. The interaction between the outgoing primary electron and the excited electron may be included to some approximation in the calculation of  $\psi_f$ .

For delocalized valence excitations, it is necessary to perform the integrals in Eq. 3 over the entire surface (or bulk) unit cell. For systems which exhibit sufficient screening, the interaction potential is short-ranged, and we can be approximated by the density of the incident electron integrated over the muffin-tin sphere of the target (or absorber) atom. This is perhaps not too unreasonable an assumption for excitations of localized states (such as core electrons).

The problem is then reduced to finding the wavefunction of the incident electron in the presence of the solid.

### B. General solution for the incident electron

We wish to solve the Schrödinger equation for the incident electron in the vicinity of an absorber atom located at the origin,

$$(H - E)|\phi\rangle = 0 \quad (4)$$

where  $|\phi\rangle$  is an eigenstate of the Hamiltonian

$$H = H_0 + V. \quad (5)$$

The solid potential  $V$  is approximated by a finite cluster of muffin-tin potentials  $V = V_a + V_N$ , where  $V_a$  is the potential of the absorber atom and

$$V_N = \sum_{n=1}^N V_n \quad (6)$$

is the sum of muffin-tin potentials  $V_n$  located at positions  $\mathbf{R}_n$ . The total number of atoms in the cluster, including the absorber, is  $N+1$ . In the region between muffin-tin spheres, the potential is constant and is taken to be the inner potential  $V_0$ , and is included in  $H_0$ ,

$$H_0 = -\frac{1}{2}\nabla^2 + V_0. \quad (7)$$

A constant  $V_0$  manifests itself in refraction of the incident beam and energy offset (reference here).

The solution of Eq. 4 can be written

$$|\phi\rangle = (1 + G_0 T)|\phi_0\rangle \quad (8)$$

where  $G_0$  is the free-space Green's propagator defined by  $(E - H_0 + i\varepsilon)^{-1}$  and  $T$  is the T-matrix for the entire system,

$$T = (t_a + t_N) + (t_a + t_N)G_0 T, \quad (9)$$

such that  $T|\phi_0\rangle = (V_a + V_N)|\phi\rangle$ . The state vector  $|\phi_0\rangle$  corresponds to the solution of the associated homogeneous equation

$$H_0|\phi_0\rangle = E|\phi_0\rangle. \quad (10)$$

In the region between muffin-tin spheres, the incident electron wave function is given by the Lippman-Schwinger equation.

$$\phi(\mathbf{k}, \mathbf{r}) = \phi_0(\mathbf{k}, \mathbf{r}) + \langle \mathbf{r} | G_0 T | \phi_0 \rangle, |\mathbf{r}| > R_{MT}. \quad (11)$$

Within the muffin-tin, the wave function must include the interaction with the absorber potential

$$\phi(\mathbf{k}, \mathbf{r}) = \phi_a(\mathbf{k}, \mathbf{r}) + \int \phi_a(\mathbf{k}', \mathbf{r}) \langle \mathbf{k}' | G_0 t_N (1 + G_0 T) | \phi_0 \rangle d\mathbf{k}', |\mathbf{r}| < R_{MT} \quad (12)$$

where  $\phi_a(\mathbf{k}, \mathbf{r})$  is the solution to the Schrödinger equation for the electron in the presence of the absorber atom alone,

$$|\phi_a\rangle = (1 + G_0 T_a) |\phi_0\rangle, \quad (13)$$

where  $T_a$  is the T-matrix for the absorber atom, defined such that  $T_a |\phi_0\rangle = V_a |\phi_a\rangle$ .  $\phi_a$  is an eigenstate of the Hamiltonian  $H_a = H_0 + V_a$  with energy  $E$  and wave vector  $\mathbf{k}$ , and can be taken from the atomic result

$$\phi_a(\mathbf{k}, \mathbf{r}) = \frac{4\pi}{k} \sum_L i^\ell e^{-i\delta_\ell^n} Y_L^*(\Omega_{\mathbf{k}}) R_\ell(\mathbf{r}) Y_L(\mathbf{r}), \quad (14)$$

where  $R_\ell(\mathbf{r})$  is the solution to the radial equation. The T-matrix elements are  $t_N = \sum_n t_n$ , where  $t_n = \sum_\ell (2\ell + 1) e^{i\delta_\ell^n} \sin(\delta_\ell^n)$ , and the  $\delta_\ell^n$  are the scattering phase shifts for the atom located at  $\mathbf{R}_n$ . Equations 11 and 12 are exact.

### C. Multiple-scattering theory

A common approach to solving this equation is given by the Dyson equation

$$GT = \sum_i G_0(\mathbf{r}, \mathbf{R}_i) t(\mathbf{R}_i) + \quad (15)$$

$$\sum_{j \neq i} \sum_i G_0(\mathbf{r}, \mathbf{R}_j) t(\mathbf{R}_j) G_0(\mathbf{R}_j, \mathbf{R}_i) t(\mathbf{R}_i) + \dots \quad (16)$$

We expand the incident electron wavefunction  $\phi(\mathbf{r})$  in a multiple scattering series

$$\phi(\mathbf{r}) = \phi^0(\mathbf{r}) + \phi^1(\mathbf{r}) + \phi^2(\mathbf{r}) + \dots + \phi^N(\mathbf{r}) \quad (17)$$

where successive terms represent no scattering, single scattering, double scattering, etc. In the limit as  $N \rightarrow \infty$ ,  $\phi(\mathbf{r})$  represents the solution to the time-independent Schrödinger equation in the presence of the solid potential. For a finite cluster of  $N$  atoms

$$\phi(\mathbf{r}) = \phi^0(\mathbf{r}) + \sum_{i=1}^N \phi^0(\mathbf{R}_i) f(\theta_s) \frac{e^{i\rho_i}}{\rho_i} e^{\rho_i/\lambda} \quad (18)$$

where the  $\mathbf{R}_i$  are bond vectors of the  $N$  lattice atoms in the cluster surrounding the absorber at  $\mathbf{R}_a$ .

#### D. Plane-wave approximation

For high-energy electrons and long bond distances such that  $kr \gg 1$ , we utilize the usual asymptotic scattering formula

$$f(\theta) = \sum_{\ell} (2\ell + 1) e^{i\delta_{\ell}} \sin(\delta_{\ell}) P_{\ell}(\cos(\theta)) \quad (19)$$

#### E. Separable propagator representation

At low energies and/or short bond distances, the expression for the scattering amplitude in Eq. 19 is inappropriate. The sphericity of the wave front becomes important. To obtain an expression for the single-scattering amplitude, we insert complete sets of states in the displaced spherical wave basis

$$\langle \mathbf{r} | k, L; \mathbf{R} \rangle \equiv i^{\ell} j_{\ell}(k|\mathbf{r} - \mathbf{R}|) Y_{\ell}^m(\Omega_{\mathbf{r}-\mathbf{R}}) \quad (20)$$

This functional form is valid only in the region of constant potential between muffin-tin spheres.

and the single-scattering amplitude reduces to

$$\phi^1(\mathbf{r}) = \sqrt{4\pi} \sum_i \sum_L G_{0L}(\rho_{\mathbf{r}_i}) t_{\ell}^i Y_L^*(\mathbf{k}) e^{i\mathbf{k} \cdot \mathbf{R}_i} \quad (21)$$

What remains is to calculate the free-space Green's function propagator  $G_{LL'}$ . We choose to express  $G$  in the separable representation of Rehr and Albers in which  $G$  is expanded in the quasi-angular momentum series

$$G_{LL'}(\rho) = \frac{e^{i\rho}}{\rho} \sum_{\lambda} \tilde{\Gamma}_{\lambda}^L(\rho) \Gamma_{\lambda}^{L'}(\rho) \quad (22)$$

Define the "Introduction Matrix"

$$\mathbf{P}_{\lambda}(\rho, \hat{\mathbf{k}}) = \sqrt{4\pi} \sum_L \Gamma_{\lambda}^L(\rho) t_{\ell} Y_L^*(\mathbf{k}) \quad (23)$$

the "Scattering Matrix"

$$\mathbf{F}_{\lambda\lambda'}(\rho, \rho') = \sum_L \Gamma_\lambda^L(\rho) t_\ell \tilde{\Gamma}_{\lambda'}^L(\rho') \quad (24)$$

and the "Termination Matrix"

$$\mathbf{M}_\lambda(\rho) = \tilde{\Gamma}_\lambda^0(\rho) \quad (25)$$

The scattering matrix is the same as that defined for the MS treatment of EXAFS and PED. The only difference in ESWSD is in the treatment of the incoming wave and the detection point. Calculations of LEED, EXAFS, and PED utilize different introduction and termination matrices, but otherwise the calculations are performed in the same manner.

### III. EXPERIMENT

Our measurements were carried out in an ultrahigh-vacuum system (base pressure  $2 \times 10^{-10}$  torr) equipped with a rotating sample mount, a pulsed low energy (5-100 eV) electron gun (pulse width 1  $\mu$ s), and a time-of-flight (TOF) mass spectrometer with unit mass resolution. Figure 1(b) is a schematic of the experimental geometry. We have chosen Cl-terminated Si(111) as a model system for this study, since the surface structure and electronic properties are well-known. The n-type Si(111) substrates were cleaned in situ by heating to 1300C for 10 seconds to desorb the oxide layer, then were cooled to 450C for deposition. The hot substrates were exposed to  $1 \times 10^{-7}$  torr of Cl<sub>2</sub> for 1000 seconds. Previous studies have shown that these preparation conditions yield a well-ordered (11) surface terminated by one monolayer (ML) of Cl atoms [ ]. The sample was mounted such that the parallel component of the electron k-vector pointed in the substrate direction (a mirror plane) at azimuth  $f = 0$ . The electron gun has a fixed 45 polar angle of incidence relative to the sample normal. Data were acquired by leaving the electron gun and TOF spectrometer fixed, while the sample was rotated in azimuth. To ensure total ion collection, an extraction field pulse of -125 V was applied between the sample and the TOF entrance grid immediately following the electron pulse. The desorption rate was measured by integrating the area under the Cl+ TOF peak. The electron energy threshold for producing

$\text{Cl}^+$  ions was measured to be 17 eV. To minimize contributions to the fine-structure from secondary electrons, data were acquired as close to the threshold energy as possible, in the range of 20 - 40 eV.

#### IV. DISCUSSION

There are some important differences between ESW-SD and other surface-sensitive electron diffraction techniques. In LEED, the interference takes place at a detector located at infinity, and the source (direct) wave does not contribute to the signal. Since the interference of the scattered waves is detected so far away, the final signal receives contributions from a large area of the surface. As a consequence, calculations of LEED intensities require summing scattered amplitudes from a large surface area. In this situation, the long-range periodicity and order of the surface is of tantamount importance. In ESW-SD, the interference takes place at the surface. The direct wave does contribute in this case, and since the inelastic mean-free path is relatively short in the energy range of interest ( $\sim 20 \text{ \AA}$  for  $E = 10 - 100 \text{ eV}$ ), only scattering from nearest neighbors within a few mean-free paths will contribute. In this case, a cluster-based calculation is appropriate, and the short-range order takes precedence over the long-range order of the surface. The interference is local, then, and is similar to that observed from photoelectron diffraction (PED). In fact, ESW-SD can be best thought of as time-reversed PED, with the important difference that the direct wave is a plane wave instead of a spherical wave. The biggest difference between ESW-SD, LEED, and PED is that ESD is often sensitive to desorption from minority sites such as step edges and defects, which are not easily observed in LEED or PED. The use of ESW-SD as a clean-surface structural probe is limited, then, to those systems in which defect and step desorption yields are small compared to terrace yields. On the other hand, ESW-SD of systems in which the signal is dominated by defects or steps offers us an unprecedented opportunity to investigate, in detail, the atomic structure of such minority sites on surfaces.

Since threshold measurements are often used to determine excitation mechanisms, the

effect of diffraction in the near-threshold region should be very important, although the 20 or so variation in amplitude should not be enough to completely wash out the threshold.

**A. Secondary electron emission**

**B. Auger electron spectroscopy**

Perhaps the most common electron-based elemental analysis technique is Auger electron spectroscopy. One directs a high-energy ( $> 1$  keV) beam of electrons at a sample and collects the spectrum of secondary electrons  $N(E)$ .

## REFERENCES

<sup>1</sup> M. P. Seah and W. A. Dench, Surf. Interface Anal. **1**, 2 (1979).

<sup>2</sup> C. Davisson and L. H. Germer, Phys. Rev. **30**, xxx (1927).

<sup>3</sup> e-2e papers.

<sup>4</sup> Pendry's LEED book, plus other references.

<sup>5</sup> Review of LEED.

<sup>6</sup> F. Peeters, E. R. Puckrin, and A. J. Slavin, J. Vac. Sci. Technol. A **8**, 797 (1990).

## FIGURES

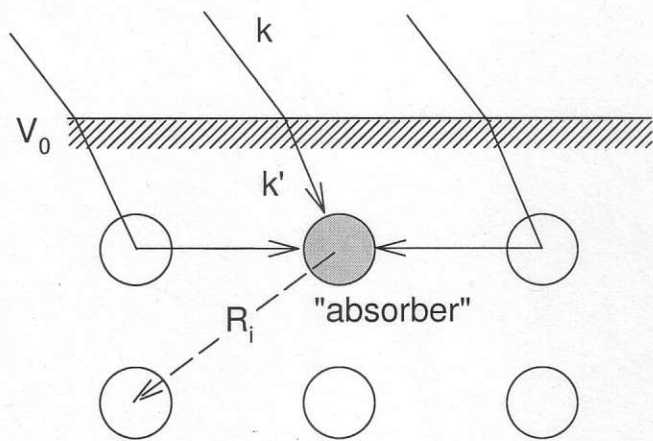


FIG. 1. Schematic diagram illustrating the ESW concept.

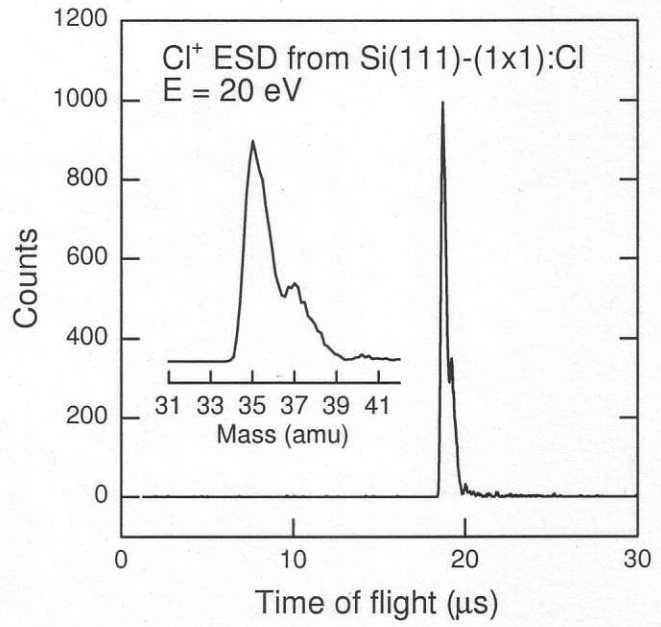


FIG. 2. Time-of-flight spectrum for Cl<sup>+</sup> ESD from Si(111)-(7x7):Cl.

*Mars*  
 The Cl<sup>-</sup> and Cl<sup>+</sup> isotope peaks are resolved.

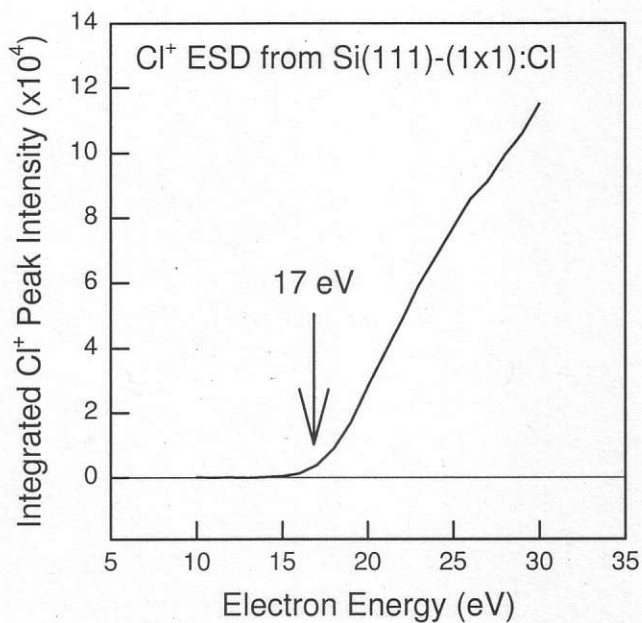


FIG. 3. Cl<sup>+</sup> ion emission intensity versus incident electron energy, showing threshold energy of 17 eV.

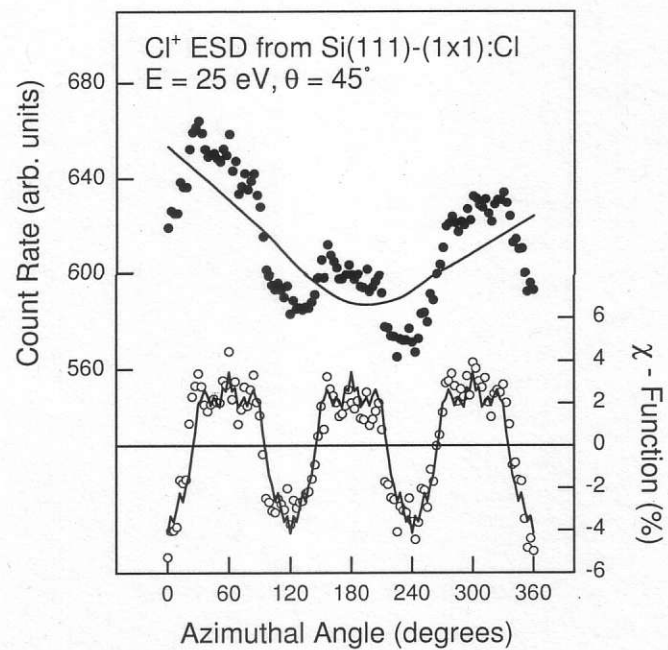


FIG. 4. Total  $Cl^+$  ion yield measured as a function of sample azimuth for a fixed polar angle of incidence  $\theta = 45^\circ$ , and an electron energy of 25 eV. Top: Raw data (circles), with a smooth fitted  $I_0$  curve (solid line). Bottom: Raw data (circles) and symmetry-averaged (solid line)  $\chi$  function.

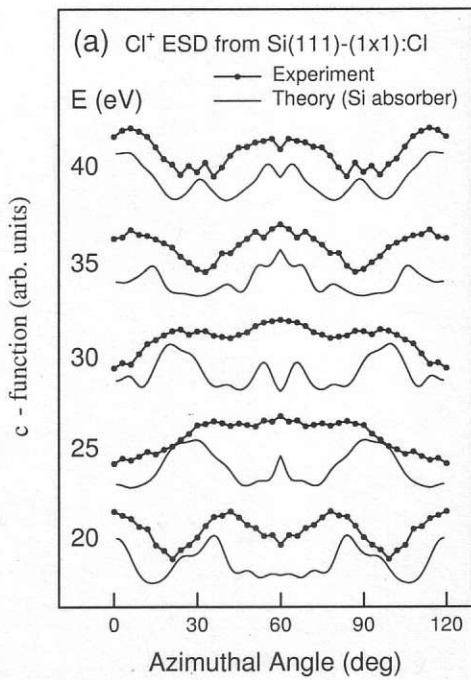


FIG. 5. Symmetry-averaged  $\chi$  functions measured at several incident electron energies, with single-scattering cluster calculations for an Si absorber.

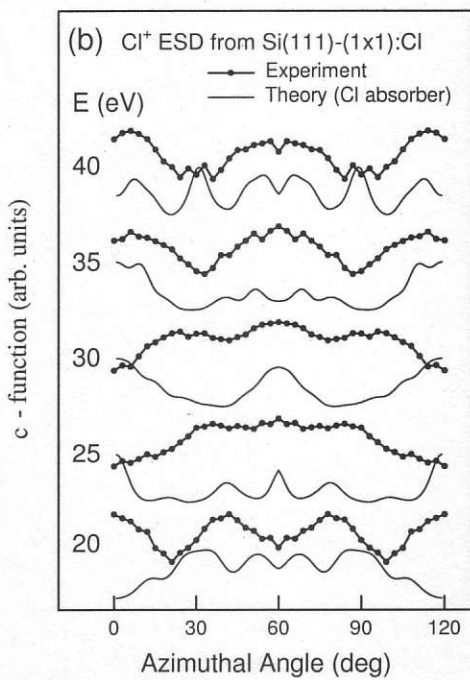


FIG. 6. Symmetry-averaged  $\chi$  functions measured at several incident electron energies, with single-scattering cluster calculations for an Cl absorber.

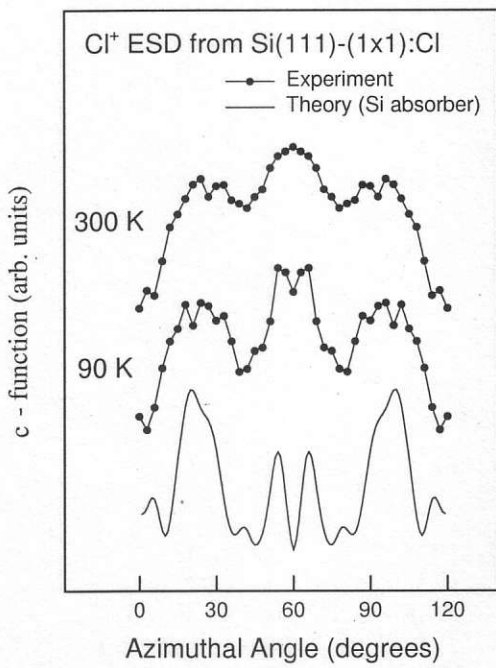


FIG. 7.  $\chi$  functions for  $E = 30$  eV at room temperature (top) and at 90 Kelvins (bottom), compared with theory at 0 K (solid line).